

Self-Assembled Supramolecular Hybrid of Carbon Nanodots and Polyoxometalates for Visible-Light-Driven Water Oxidation

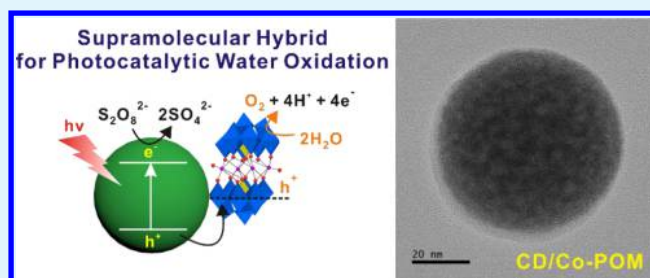
Yuri Choi,^{†,§} Dasom Jeon,^{‡,§} Yeongkyu Choi,[†] Jungki Ryu,^{*,‡} and Byeong-Su Kim^{*,†,‡}

[†]Department of Chemistry and [‡]Department of Energy Engineering, Ulsan National Institute of Science and Technology (UNIST), Ulsan 44919, Republic of Korea

Supporting Information

ABSTRACT: Water splitting is considered the most attractive pursuit in the field of solar energy conversion. In this study, we report the synthesis and application of a supramolecular hybrid of carbon nanodot (CD) and cobalt polyoxometalate (Co-POM) to solar water oxidation. The self-assembly of the alginate-based CD and Co-POM led to the formation of a spherical hybrid of CD/Co-POM. Owing to the facile transfer of photogenerated holes from CD under visible light irradiation, the hybrid donor–acceptor type of CD/Co-POM enabled the rapid scavenging of holes and accumulation of a long-lived oxidation state of Co-POM for efficient solar water oxidation, outperforming conventional [Ru(bpy)₃]²⁺-based systems. We believe that this study offers new insights into the development of CD-based nanocomposites with various photocatalytic and optoelectronic applications.

KEYWORDS: photocatalyst, carbon nanodot, polyoxometalate, self-assembly, oxygen evolution



INTRODUCTION

Water splitting is considered the most attractive pursuit in the field of solar energy conversion to address current energy and environmental issues.^{1,2} To date, various semiconducting materials (e.g., metal oxides and chalcogenides) have been used for solar water splitting;³ however, many of these materials have limited utility because they contain rare, expensive, or toxic elements.^{4,5} Significant advances have been recently made to overcome these challenges, including the development of efficient and cost-effective materials.^{6–8} In addition, integration with charge carrier acceptors, such as metal nanoparticles and graphene, and co-catalysts can facilitate electron/hole transport within the semiconducting materials and electrocatalytic reactions, respectively.^{9–11} Nevertheless, overcoming inherent problems such as harsh synthetic conditions, a narrow pH window for reliable operation, and low stability continue to be challenging endeavors.^{6–8}

Recently, carbon nanodots (CDs) have emerged as a new class of light-harvesting materials with notable advantages, including strong and broad optical absorption, high chemical stability, excellent electron- and hole-transfer capability, and low toxicity.^{12–14} Moreover, CDs can easily be prepared under mild conditions from abundant and renewable biomass resources.^{15–17} Thus far, CD-based hybrid nanomaterials have demonstrated good photocatalytic efficiency for the oxidative degradation of pollutants or reductive production of hydrogen.^{18–21} Despite these excellent examples, the application of CDs in photocatalytic water oxidation is still limited due to difficulties in the photogeneration and accumulation of the long-lived oxidation state required for a slow four-electron

water oxidation process.²² Recently, it has been reported that such issues can be addressed by forming CD-based heterojunction or composite structures.²³ However, complex and less environmentally tolerant processes are still required, such as the use of toxic chemicals and high-temperature processes in addition to generation of corrosive hydrogen peroxide as a reaction intermediate.

In this context, polyoxometalates (POMs) with an oxo-bridged polynuclear transition metal complex have been suggested as both fast hole-scavengers and effective water oxidation catalysts. POMs can undergo fast and reversible multielectron-transfer reactions without altering their structures.^{24–27} Moreover, owing to their highly negative surface charges, POMs can be used as building blocks for the self-assembly of supramolecular hybrid nanomaterials.^{28–31}

Herein, we report the synthesis of supramolecular hybrid colloidal nanocomposite by exploiting the self-assembly of CD and POM for highly efficient water oxidation under visible light irradiation (Figure 1). In particular, nontoxic, cost-effective, and earth-abundant nanomaterials, namely, alginate-based CD and POM with a tetracobalt active site [Co₄(H₂O)₂(PW₉O₃₄)₂]^{10–} (Co-POM), were selected as the photosensitizer and water oxidation catalyst for the formation of a donor–acceptor-type hybrid nanostructure. A spherical donor–acceptor-type CD/Co-POM hybrid was readily synthesized by self-assembly and exhibited excellent performance for photocatalytic water

Received: January 4, 2018

Accepted: April 6, 2018

Published: April 6, 2018



Figure 1. (a) Preparation of supramolecular hybrid CD/Co-POM structure for photocatalytic water oxidation. (b) Band diagram of CD and Co-POM.

oxidation. A series of spectroscopic analyses, including UV–vis, photoluminescence (PL), Fourier transform infrared (FT-IR), and X-ray photoelectron spectroscopy (XPS), confirmed the successful formation of an efficient donor–acceptor hybrid, which facilitated fast transfer of photogenerated holes from CD to POM. As a result, the supramolecular CD/Co-POM hybrid achieved outstanding performance for photocatalytic oxygen evolution with a significantly higher turnover number (TON) than that of typical systems based on $[\text{Ru}(\text{bpy})_3]^{2+}$ that are widely known to possess excellent photophysical properties.³² We anticipate that this study will lead to the development of new types of self-assembled photocatalysts in various photocatalytic and optoelectronic applications.

EXPERIMENTAL METHODS

Synthesis of CD and Co-POM. For the preparation of CD, 9 mg of alginate (0.052 mmol, Sigma-Aldrich) was dissolved in 10 mL of water and 600 μL of 1.0 M HCl was added.³³ The solution was then mixed with 694 μL of ethylenediamine (10.4 mmol) with vigorous stirring for 2 min. The solution was placed in a microwave oven

(Samsung MS-23F301TAW, 700W) and heated for 2 min. After cooling to room temperature, a red-brown solid was obtained, which was dissolved in 2 mL of water and filtered through a syringe filter (0.45 μm) to remove salts and unreacted alginate. The tetracobalt-substituted POM catalyst (Co-POM) was synthesized according to the method described in the literature.²⁴

Synthesis of the Supramolecular Hybrid of CD/Co-POM.

CD/Co-POM composite was prepared by simply mixing an aqueous solution of Co-POM (15 μM) with CD solutions of various concentrations (0.10–5.0 mg/mL) in borate buffer (80 mM, pH 8.0).

Characterization. A UV/vis spectrophotometer (UV-2550, Shimadzu) was used to record the absorption spectra of CD and Co-POM. The highest occupied molecular orbital (HOMO) level of CD was evaluated by ultraviolet photoelectron spectroscopy (ESCALAB 250XI, Thermo Fisher). A fluorescence spectrometer (RF-6000, Shimadzu) was used to measure the emission spectra of CD and CD/Co-POM. The ζ potential of the colloidal suspensions was measured using a ζ potential analyzer (Malvern, Zetasizer Nano ZS). The structure of the CD/Co-POM was analyzed by FT-IR (Cary 660, Varian), X-ray photoelectron spectroscopy (XPS, Cu $K\alpha$ radiation, Thermo Fisher), and Raman (alpha300R, WITec) spectroscopy. The morphology and size of CD/Co-POM were examined using high-

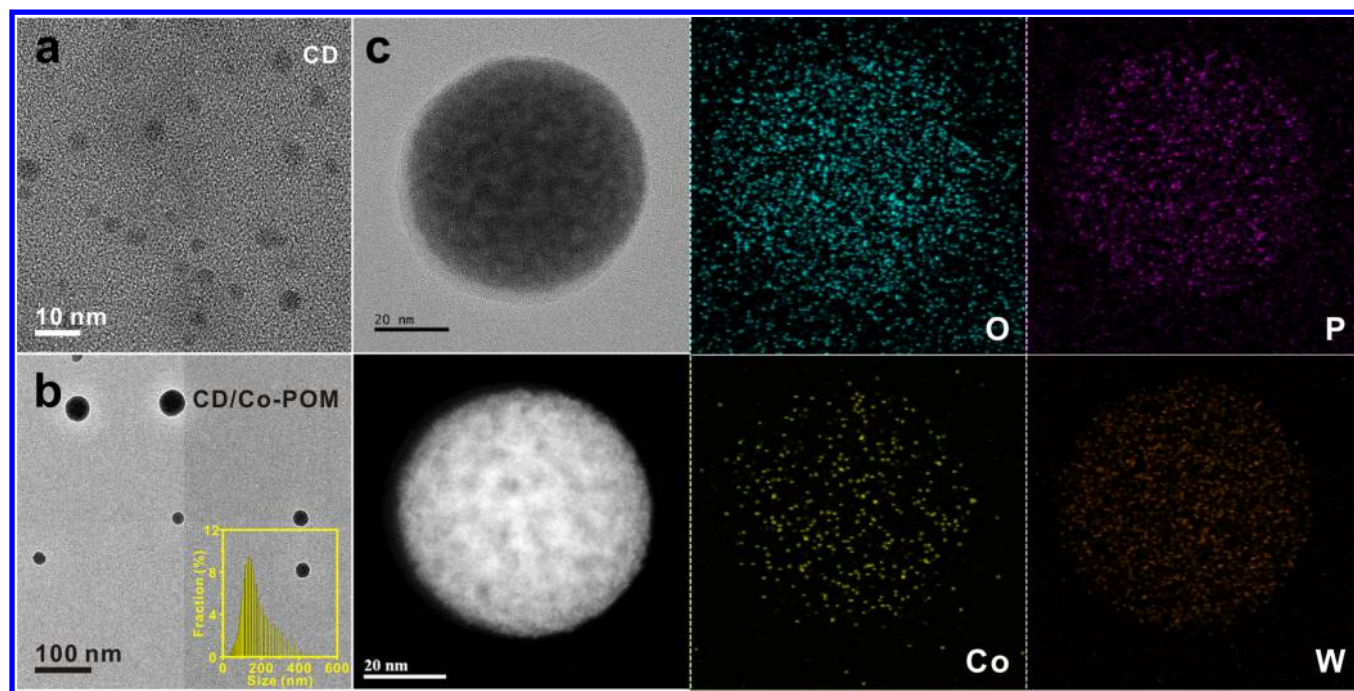


Figure 2. Transmission electron microscopy (TEM) images of (a) CD and (b) CD/Co-POM prepared with 0.50 mg/mL of CD and 15 μ M Co-POM. The inset shows the size distribution of CD/Co-POM determined by dynamic light scattering. (c) HR-TEM and high-angle annular dark-field scanning TEM images of CD/Co-POM with the corresponding elemental mapping images.

resolution transmission electron microscopy (HR-TEM), high-angle annular dark-field scanning TEM, and energy-dispersive X-ray spectroscopy (JEOL, JEM-2100F, accelerating voltage of 200 kV). Size distribution analysis was performed using dynamic light scattering (BI-APD, Brookhaven Instruments, New York). Picosecond-resolved fluorescence decay profiles were measured using a time-correlated single-photon counting (TCSPC) spectrometer (FluoTime 300, PicoQuant). Cyclic voltammetry (CV) was carried out using a potentiostat/galvanostat (MWPG1000, WonATech) under the following conditions: Ag/AgCl as the reference electrode, Pt wire as the counter electrode, and a glassy carbon electrode as the working electrode in a 0.1 M sodium phosphate buffer (pH 7) at a scan rate of 25 mV/s. CD/Co-POM (10 μ L) and Nafion solution (10 μ L) were dropped and dried on the glass carbon electrode.

Photocatalytic Experiment. Photocatalytic oxygen evolution was carried out in a 20 mL glass vial containing 2 mL of the CD/Co-POM solution. Prior to the experiment, the vial was sealed with a rubber septum and purged with nitrogen for 30 min. Sodium sulfate (0.15 M) was used as a sacrificial electron acceptor. The CD/Co-POM solution was vigorously stirred under visible light irradiation (300 W Xe lamp) with a 400 nm cutoff filter and an IR water filter. The evolution of oxygen from the solution was determined using gas chromatography (GC-2010 Plus, Shimadzu).

RESULTS AND DISCUSSION

Co-POM with excellent catalytic activity and low overpotential for water oxidation was prepared according to a previous report.²⁴ The as-prepared Co-POM showed a unique absorption band at 579 nm (Figure S1). In parallel, the yellow suspension of CD was readily synthesized by microwave-assisted pyrolysis of the alginate precursor in the presence of ethylenediamine as a surface-passivating agent and HCl as a solubilizing agent.³³ Interestingly, the prepared CD exhibited a broad absorption band above 400 nm (Figure S1). A characteristic blue emission was observed with the maxima strongly dependent on the excitation wavelength with a quantum yield of 10%. We chose alginate-derived CD because

of its excellent electron- and hole-donating ability under irradiation (Figure S2).

When CD was mixed with Co-POM, clusters of CD/Co-POM were formed immediately and produced a stable suspension, which changed color from yellow to turbid white, indicating the formation of a self-assembled nanostructure (Figures 1a and S1). This suspension was stable without noticeable precipitation for several months. Moreover, after addition of Co-POM, the ζ potential value of the CD suspension decreased from -18.2 ± 0.6 to -35.1 ± 0.2 mV due to self-assembly with the Co-POM bearing a highly negative surface charge (-42.4 ± 4.6 mV), suggesting association based on the electrostatic interaction between CD and Co-POM.

To confirm its potential as a water oxidation photocatalyst in this system, the band-edge position of CD was determined by the Tauc plot and ultraviolet photoelectron spectroscopy^{23,34} and the onset potential for water oxidation by Co-POM was measured by cyclic voltammetry (CV) (Figures 1b and S3). The calculated band gap, HOMO, and lowest unoccupied molecular orbital of CD were determined to be 2.89, 7.78 (3.34 vs reversible hydrogen electrode (RHE)), and 4.89 eV vs vacuum (0.45 vs RHE), respectively. The HOMO level of CD was more positive than the thermodynamic redox potential for water oxidation (1.23 V vs RHE) and the onset potential for water oxidation by Co-POM (1.769 V vs RHE at pH 8), thus providing the optimum band gap and band-edge position for an effective water oxidation reaction.

The unique morphology of CD and CD/Co-POM was characterized by HR-TEM. The average diameter of CD was measured to be 10 nm (Figure 2a); interestingly, however, the hybrid CD/Co-POM displayed a spherical nanostructure with an average diameter of 51 ± 14 nm (Figures 2b and S4). The dynamic light scattering measurement also indicated the formation of nanocomposites with an average hydrodynamic

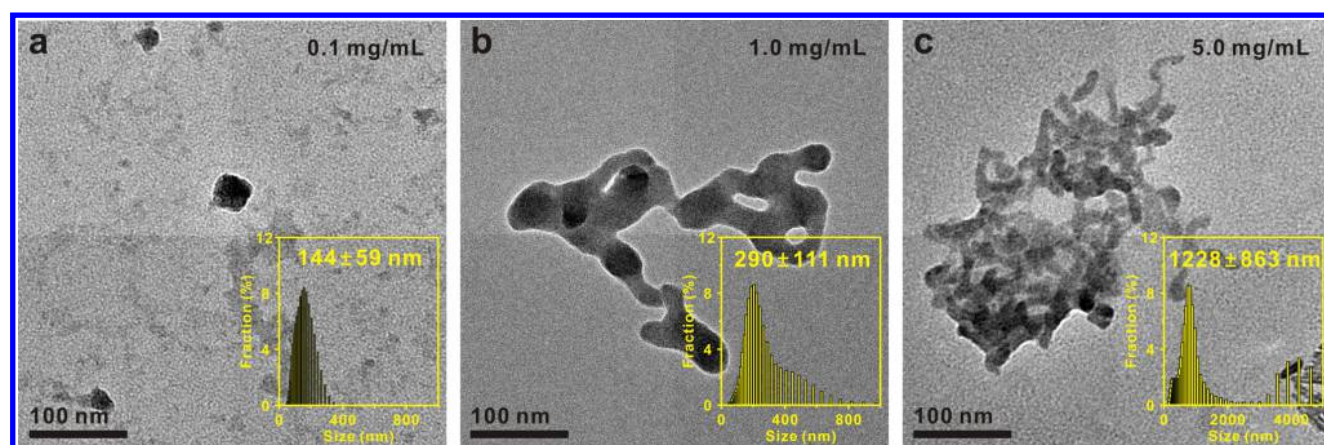


Figure 3. TEM images of CD/Co-POM prepared with (a) 0.10 mg/mL, (b) 1.0 mg/mL, and (c) 5.0 mg/mL of CD at a fixed concentration of Co-POM (15 μ M). The insets show the size distribution of CD/Co-POM measured by dynamic light scattering.

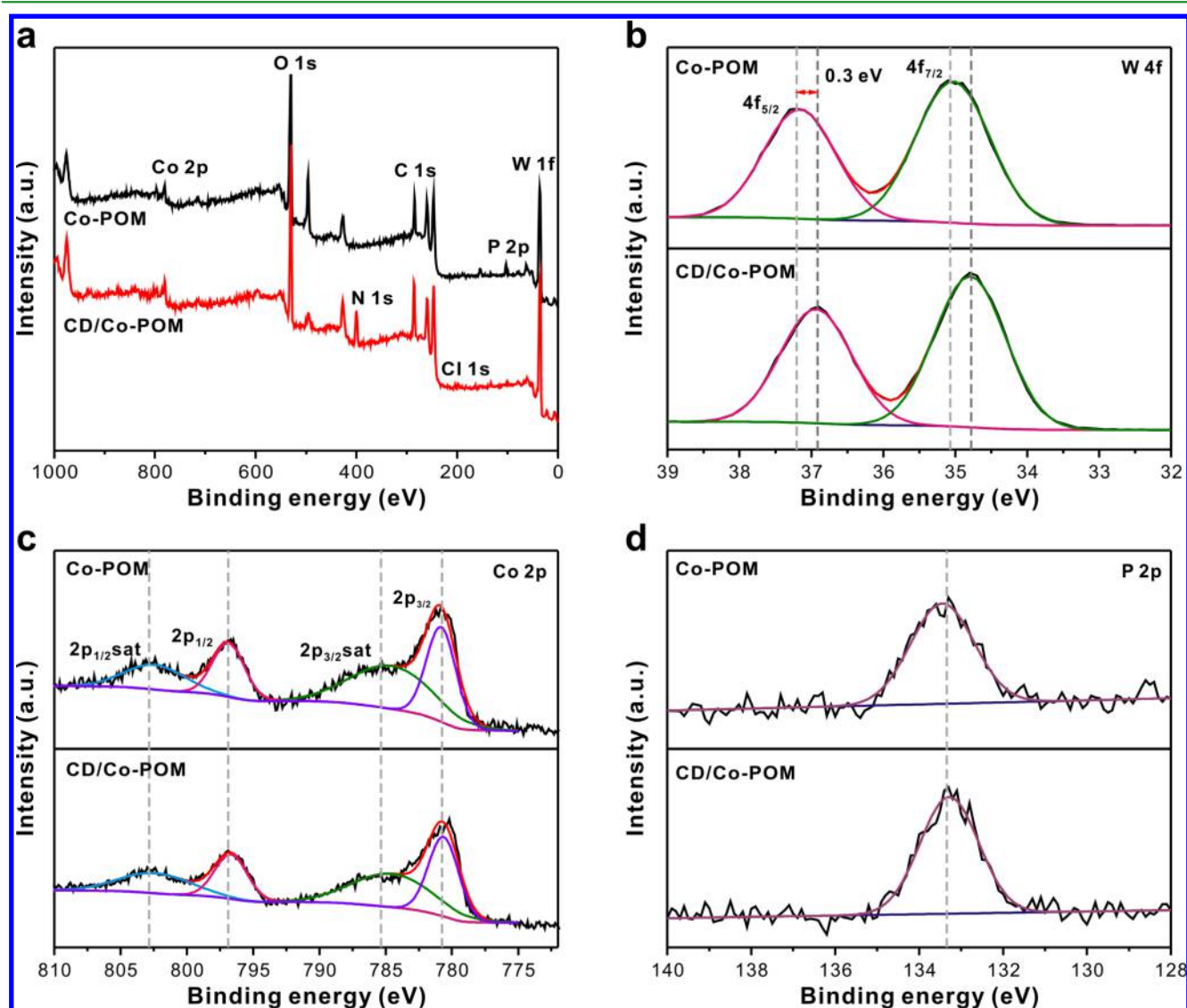


Figure 4. (a) XPS survey spectra of Co-POM and CD/Co-POM. (b–d) High-resolution X-ray photoelectron spectra of Co-POM and CD/Co-POM with the corresponding deconvoluted elemental peak positions for (b) W 4f, (c) Co 2p, and (d) P 2p.

diameter of 126 ± 61 nm. High-angle annular dark-field scanning TEM images suggested a homogeneous distribution of the respective elements of Co-POM, such as Co, P, and W,

within the composite (Figure 2c). Given their distinctive size differences, this observation illustrates that the spherical hybrid

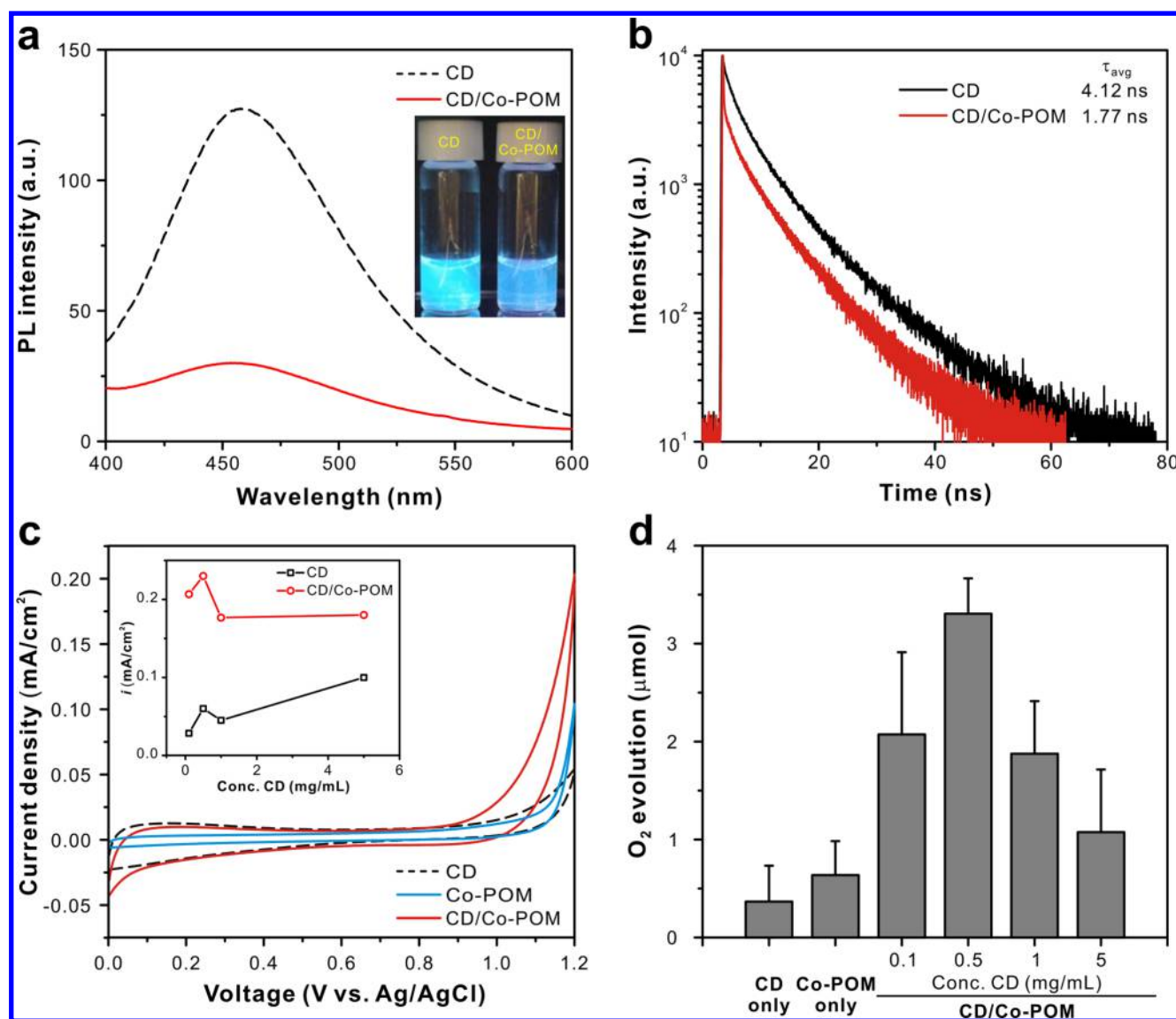


Figure 5. Photocatalytic oxygen evolution of hybrid CD/Co-POM. (a) PL spectra of CD (dashed) and CD/Co-POM (solid). (b) PL decay profiles of CD and CD/Co-POM characterized by time-correlated single-photon counting (TCSPC) spectroscopy at $\lambda_{ex} = 375$ nm and $\lambda_{em} = 450$ nm. (c) Cyclic voltammetry of CD (black, dashed), Co-POM (blue, solid), and CD/Co-POM (red, solid). The scan rate is 25 mV/s in 0.10 M sodium phosphate at pH 7. The concentration of CD is 0.50 mg/mL. The inset in (c) shows the current density at 1.2 V for different CD concentrations. (d) Oxygen evolution from CD, Co-POM, and CD/Co-POM composite with different CD concentrations under visible light irradiation with a 400 nm cutoff filter for 20 min.

CD/Co-POM nanostructure was composed of self-assembled clusters of CD and Co-POM.

The structure of hybrid CD/Co-POM was further optimized by varying the relative concentration of CD at a fixed concentration of Co-POM (0.84 mg/mL, 15 μ M). The self-assembled hybrid structures were observed for all CD concentrations tested (0.10–5.0 mg/mL); interestingly, a spherical structure was observed only when 0.50 mg/mL of CD was used, whereas aggregated structures were found with increasing CD concentration (Figure 3). In all cases, elemental mapping showed that Co-POM was evenly distributed throughout the composite (Figure S5).

The formation of the CD/Co-POM composite was further supported by XPS and FT-IR measurements. The deconvoluted C 1s and N 1s X-ray photoelectron spectra indicated the presence of oxygen and nitrogen-based functional groups in CD, which were derived from the precursor and served as

interaction sites with Co-POM (Figure S6). After the supramolecular self-assembly process, the elemental components of CD and Co-POM, such as C, O, Co, P, and W, were observed in CD/Co-POM (Figure 4a and Table S1). A comparison of the elemental ratios of Co-POM showed that the W/Na ratio increased significantly after the formation of the supramolecular CD/Co-POM nanocomposite, indicating the substitution of Na⁺ present in Co-POM with CD through electrostatic interactions (Table S2). Most notably, the W 4f peaks shifted to a lower binding energy by 0.3 eV, suggesting an interaction between CD and the WO₆ octahedra in Co-POM (Figure 4b). In contrast, no shift in the Co 2p and P 2p peaks was observed, highlighting that the structure of the photocatalytic active site of Co-POM remained intact even after the formation of the supramolecular hybrid composite (Figure 4c,d). In agreement with the XPS results, the characteristic FT-IR peaks of Co-POM in the hybrid CD/Co-POM sample

shifted to 1027 (P–O), 933 (W=O_v, terminal), 882 (W–O_c–W, corner sharing), 781 (W–O_e–W, edge sharing), and 722 (W–O_b–W, sandwich bound) cm⁻¹ (Figure S7). These results show that the hybrid composite self-assembled by electrostatic and hydrogen-bonding interactions between WO₆ octahedra in Co-POM and the abundant functional groups in CD.²⁹ As a control set, analysis of cobalt-free POM (Na₉(PW₉O₃₄)) and CD hybrid nanocomposite assembled in a similar manner further supported a specific molecular interaction independent of the Co center (Figure S8).

The PL spectrum and CV graph of the CD were measured before and after self-assembly with Co-POM. The PL intensity of CD/Co-POM decreased by 72% compared to that of CD alone, indicating the efficient transfer of the photoexcited charge carriers from CD to Co-POM due to their close association (Figure 5a). In agreement with these results, PL lifetime was also significantly reduced from 4.12 ns in CD to 1.77 ns in CD/Co-POM, which was characterized by time-correlated single-photon counting (TCSPC) spectroscopy (Figure 5b and Table S3). Furthermore, CV confirmed the more efficient transfer of charge carriers from CD to water in the presence of Co-POM (Figure 5c). When CD self-assembled with Co-POM, the current density increased by approximately 2-fold due to the efficient transfer of charge carriers between CD and Co-POM and high catalytic activity of Co-POM for water oxidation. We further optimized the current density by controlling the concentration of CD with respect to Co-POM (Figures 5c and S9). The highest current density was observed at a CD concentration of 0.50 mg/mL, which also supported the enhanced electron/hole transfer attributed to the well-defined spherical structure shown in the TEM images. The observed behavior can be also explained by assuming that there is an optimum ratio between the photosensitizer (i.e., CD) and water oxidation catalyst (i.e., Co-POM)²⁴ and that electrocatalytic oxidation of water is the rate-determining step in the overall photocatalytic water oxidation reaction.³⁵

The chemical identity of the active site of CD/Co-POM was further confirmed by the Raman and X-ray photoelectron spectra before and after visible light irradiation for 1 h for photocatalytic water oxidation (Figure S10). Although the decomposition of Co-POM to CoO_x in the electrocatalytic system was often observed,³⁶ we could not observe the strong Raman peaks associated with CoO_x or Co₃O₄ in photochemical water oxidation.²⁵ This is in accord with the recent study by Schiwon et al. who demonstrated the absence of hydrolytic or oxidative transformation of Co-POM based on X-ray absorption fine structure spectroscopy.²⁷ Furthermore, the Co 2p peaks did not shift after visible light irradiation in the X-ray photoelectron spectra. Taken together, these results verified that Co-POM was indeed responsible for the photocatalytic activity of the system.

Finally, to evaluate the photocatalytic activity of CD/Co-POM as a water oxidation catalyst, oxygen evolution under visible light irradiation was determined by gas chromatography. Water oxidation was performed using different concentrations of CD as a photosensitizer in borate buffer solution with Na₂S₂O₈ as a sacrificial electron acceptor. The amount of oxygen evolved from CD/Co-POM was dependent on the irradiation time (Figure S11). In agreement with the cyclic voltammetry data, the amount of oxygen generated from CD also increased significantly upon association with Co-POM, with up to 6 times (2.4 μmol) more oxygen generated at a CD concentration of 0.50 mg/mL (Figure 5d). At this concen-

tration, the TON for oxygen evolution was determined to be 552, which might be limited by consumption of the sacrificial electron acceptor but was still significantly higher than those from our experiment (TON = 152) under identical experimental conditions using expensive [Ru(bpy)₃]²⁺ as a photosensitizer (Table S4 and Figure S12). Notably, [Ru(bpy)₃]²⁺ has been widely used for decades in various photocatalytic applications due to its excellent photophysical properties, such as strong light absorption, high oxidation potential, and the long lifetime of its excited state.³⁷ This CD/Co-POM composite also exhibited much higher cycle stability than that of [Ru(bpy)₃]²⁺/Co-POM. Because of the high dispersity in aqueous media, which resulted in difficulties in the recovery of CD/Co-POM, we performed the recycle stability by supplying Na₂S₂O₈ as a sacrificial electron acceptor repeatedly upon photocatalytic oxygen evolution test. Although [Ru(bpy)₃]²⁺/Co-POM became quickly deactivated and lost most of its activity in the first cycle, CD/Co-POM exhibited moderate stability where 72.8% of the initial activity was maintained even after the third cycle (Figure S13). Nevertheless, further stability improvement is required for their practical application, which is currently underway in our group.

Interestingly, less oxygen was evolved for samples with a CD concentration above 5.0 mg/mL, which could be attributed to decreased charge carrier transfer within the aggregated structures (Figure S14). As a control, the Co-based water oxidation reaction was performed using the cobalt ion (Co²⁺) instead of Co-POM;³⁸ however, after 20 min, only 0.6 μmol oxygen evolved from this system (Figure S15). Furthermore, the stability of CD/Co-POM hybrid was high enough to ensure its integrity during solar water oxidation (Figure S16). These results demonstrate that the photocatalytic water oxidation efficiency was associated with the specific combination of the CD photosensitizer and Co-POM water oxidation catalyst.

CONCLUSIONS

In conclusion, we developed a self-assembled hybrid photocatalyst CD/Co-POM for visible-light-driven water oxidation. The alginate-based CD possessed abundant functional groups for assembly with the highly negatively charged Co-POM by electrostatic and hydrogen-bonding interactions to form spherical supramolecular hybrid nanocomposite. Moreover, because of the superior electron/hole-transfer properties of CD under visible light irradiation, Co-POM can accept the photoexcited hole from CD, resulting in outstanding photocatalytic oxygen evolution performance compared to conventional [Ru(bpy)₃]²⁺-based composites. We anticipate that this study provides new insights on the use of CD not only as a building block for self-assembly but also as a photosensitizer with a variety of potential applications, including water splitting, sensors, and optoelectronic devices.

ASSOCIATED CONTENT

Supporting Information

The Supporting Information is available free of charge on the ACS Publications website at DOI: 10.1021/acsami.8b00162.

UV/vis and PL spectra of CD and Co-POM; ultraviolet photoelectron spectroscopy analysis; XPS and FT-IR spectroscopy; photocatalytic water oxidation performance; performance comparison table (PDF)

AUTHOR INFORMATION

Corresponding Authors

*E-mail: jryu@unist.ac.kr (J.R.).

*E-mail: bskim19@unist.ac.kr (B.-S.K.).

ORCID

Yuri Choi: 0000-0002-4691-230X

Dasom Jeon: 0000-0002-2297-0396

Yeongkyu Choi: 0000-0001-5680-1390

Jungki Ryu: 0000-0002-0897-8463

Byeong-Su Kim: 0000-0002-6419-3054

Author Contributions

[§]Y.C. and D.J. contributed equally to this work.

Notes

The authors declare no competing financial interest.

ACKNOWLEDGMENTS

We thank Prof. Myoung Hoon Song and Seungjin Lee for assistance in TCSPC experiment. This work was supported by the National Research Foundation of Korea (NRF) grant (NRF-2015R1A2A2A04003160, 2015R1C1A1A02037698, 2017R1A6A3A11028305, and 2017M3A7B4052802).

REFERENCES

- (1) Meyer, T. J. Catalysis: The Art of Splitting Water. *Nature* **2008**, *451*, 778–779.
- (2) Kudo, A.; Miseki, Y. Heterogeneous Photocatalyst Materials for Water Splitting. *Chem. Soc. Rev.* **2009**, *38*, 253–278.
- (3) Chen, X.; Shen, S.; Guo, L.; Mao, S. S. Semiconductor-Based Photocatalytic Hydrogen Generation. *Chem. Rev.* **2010**, *110*, 6503–6570.
- (4) Frame, F. A.; Townsend, T. K.; Chamousis, R. L.; Sabio, E. M.; Dittrich, T.; Browning, N. D.; Osterloh, F. E. Photocatalytic Water Oxidation with Nonsensitized IrO₂ Nanocrystals under Visible and UV Light. *J. Am. Chem. Soc.* **2011**, *133*, 7264–7267.
- (5) Lee, J. M.; Mok, E. K.; Lee, S.; Lee, N. S.; Debbichi, L.; Kim, H.; Hwang, S. J. A Conductive Hybridization Matrix of RuO₂ Two-Dimensional Nanosheets: A Hybrid-Type Photocatalyst. *Angew. Chem., Int. Ed.* **2016**, *55*, 8546–8550.
- (6) Sivula, K.; Le Formal, F.; Grätzel, M. Solar Water Splitting: Progress using Hematite (α -Fe₂O₃) Photoelectrodes. *ChemSusChem* **2011**, *4*, 432–449.
- (7) Jang, J.-W.; Du, C.; Ye, Y.; Lin, Y.; Yao, X.; Thorne, J.; Liu, E.; McMahon, G.; Zhu, J.; Javey, A.; et al. Enabling Unassisted Solar Water Splitting by Iron Oxide and Silicon. *Nat. Commun.* **2015**, *6*, No. 7447.
- (8) Zhu, T.; Chong, M. N.; Chan, E. S. Nanostructured Tungsten Trioxide Thin Films Synthesized for Photoelectrocatalytic Water Oxidation: A Review. *ChemSusChem* **2014**, *7*, 2974–2997.
- (9) Hong, D. C.; Yamada, Y.; Nagatomi, T.; Takai, Y.; Fukuzumi, S. Catalysis of Nickel Ferrite for Photocatalytic Water Oxidation Using [Ru(bpy)₃]²⁺ and S₂O₈²⁻. *J. Am. Chem. Soc.* **2012**, *134*, 19572–19575.
- (10) Tong, H.; Ouyang, S. X.; Bi, Y. P.; Umezawa, N.; Oshikiri, M.; Ye, J. H. Nano-Photocatalytic Materials: Possibilities and Challenges. *Adv. Mater.* **2012**, *24*, 229–251.
- (11) Xiang, Q.; Cheng, B.; Yu, J. G. Graphene-Based Photocatalysts for Solar-Fuel Generation. *Angew. Chem., Int. Ed.* **2015**, *54*, 11350–11366.
- (12) Baker, S. N.; Baker, G. A. Luminescent Carbon Nanodots: Emergent Nanolights. *Angew. Chem., Int. Ed.* **2010**, *49*, 6726–6744.
- (13) Fernando, K. A. S.; Sahu, S.; Liu, Y. M.; Lewis, W. K.; Gulianti, E. A.; Jafariyan, A.; Wang, P.; Bunker, C. E.; Sun, Y. P. Carbon Quantum Dots and Applications in Photocatalytic Energy Conversion. *ACS Appl. Mater. Interfaces* **2015**, *7*, 8363–8376.
- (14) Strauss, V.; Margraf, J. T.; Dolle, C.; Butz, B.; Nacken, T. J.; Walter, J.; Bauer, W.; Peukert, W.; Spiecker, E.; Clark, T.; Guldi, D. M. Carbon Nanodots: Toward a Comprehensive Understanding of Their Photoluminescence. *J. Am. Chem. Soc.* **2014**, *136*, 17308–17316.
- (15) Li, H.; Kang, Z.; Liu, Y.; Lee, S.-T. Carbon Nanodots: Synthesis, Properties and Applications. *J. Mater. Chem.* **2012**, *22*, 24230–24253.
- (16) Zhu, S.; Song, Y.; Zhao, X.; Shao, J.; Zhang, J.; Yang, B. The Photoluminescence Mechanism in Carbon Dots (Graphene Quantum Dots, Carbon Nanodots, and Polymer Dots): Current State and Future Perspective. *Nano Res.* **2015**, *8*, 355–381.
- (17) Briscoe, J.; Marinovic, A.; Sevilla, M.; Dunn, S.; Titirici, M. Biomass-Derived Carbon Quantum Dot Sensitizers for Solid-State Nanostructured Solar Cells. *Angew. Chem., Int. Ed.* **2015**, *54*, 4463–4468.
- (18) Li, H.; He, X. D.; Kang, Z. H.; Huang, H.; Liu, Y.; Liu, J. L.; Lian, S. Y.; Tsang, C. H. A.; Yang, X. B.; Lee, S. T. Water-Soluble Fluorescent Carbon Quantum Dots and Photocatalyst Design. *Angew. Chem., Int. Ed.* **2010**, *49*, 4430–4434.
- (19) Yu, H.; Zhao, Y.; Zhou, C.; Shang, L.; Peng, Y.; Cao, Y.; Wu, L.-Z.; Tung, C.-H.; Zhang, T. Carbon Quantum Dots/TiO₂ Composites for Efficient Photocatalytic Hydrogen Evolution. *J. Mater. Chem. A* **2014**, *2*, 3344–3351.
- (20) Martindale, B.; Joliat, E.; Bachmann, C.; Alberto, R.; Reisner, E. Clean Donor Oxidation Enhances the H₂ Evolution Activity of a Carbon Quantum Dot–Molecular Catalyst Photosystem. *Angew. Chem., Int. Ed.* **2016**, *55*, 9402–9406.
- (21) Hutton, G. A. M.; Reuillard, B.; Martindale, B. C. M.; Caputo, C. A.; Lockwood, C. W. J.; Butt, J. N.; Reisner, E. Carbon Dots as Versatile Photosensitizers for Solar-Driven Catalysis with Redox Enzymes. *J. Am. Chem. Soc.* **2016**, *138*, 16722–16730.
- (22) Duan, L.; Tong, L.; Xu, Y.; Sun, L. Visible Light-Driven Water Oxidation—From Molecular Catalysts to Photoelectrochemical Cells. *Energy Environ. Sci.* **2011**, *4*, 3296–3313.
- (23) Liu, J.; Liu, Y.; Liu, N.; Han, Y.; Zhang, X.; Huang, H.; Lifshitz, Y.; Lee, S.-T.; Zhong, J.; Kang, Z. Metal-Free Efficient Photocatalyst for Stable Visible Water Splitting via a Two-Electron Pathway. *Science* **2015**, *347*, 970–974.
- (24) Yin, Q.; Tan, J. M.; Besson, C.; Geletii, Y. V.; Musaev, D. G.; Kuznetsov, A. E.; Luo, Z.; Hardcastle, K. I.; Hill, C. L. A Fast Soluble Carbon-Free Molecular Water Oxidation Catalyst Based on Abundant Metals. *Science* **2010**, *328*, 342–345.
- (25) Song, F.; Ding, Y.; Ma, B.; Wang, C.; Wang, Q.; Du, X.; Fu, S.; Song, J. K₇ [Co^{III}Co^{II}(H₂O)W₁₁O₃₉]: A Molecular Mixed-Valence Keggin Polyoxometalate Catalyst of High Stability and Efficiency for Visible Light-Driven Water Oxidation. *Energy Environ. Sci.* **2013**, *6*, 1170–1184.
- (26) Han, X.-B.; Zhang, Z.-M.; Zhang, T.; Li, Y.-G.; Lin, W.; You, W.; Su, Z.-M.; Wang, E.-B. Polyoxometalate-Based Cobalt–Phosphate Molecular Catalysts for Visible Light-Driven Water Oxidation. *J. Am. Chem. Soc.* **2014**, *136*, 5359–5366.
- (27) Schiwon, R.; Klingan, K.; Dau, H.; Limberg, C. Shining Light on Integrity of a Tetracobalt-Polyoxometalate Water Oxidation Catalyst by X-Ray Spectroscopy Before and After Catalysis. *Chem. Commun.* **2014**, *50*, 100–102.
- (28) Long, D. L.; Tsunashima, R.; Cronin, L. Polyoxometalates: Building Blocks for Functional Nanoscale Systems. *Angew. Chem., Int. Ed.* **2010**, *49*, 1736–1758.
- (29) Yan, X.; Zhu, P.; Fei, J.; Li, J. Self-Assembly of Peptide-Inorganic Hybrid Spheres for Adaptive Encapsulation of Guests. *Adv. Mater.* **2010**, *22*, 1283–1287.
- (30) Gao, P.; Wu, Y. Q.; Wu, L. X. Co-Assembly of Polyoxometalates and Peptides towards Biological Applications. *Soft Matter* **2016**, *12*, 8464–8479.
- (31) Jeon, D.; Kim, H.; Lee, C.; Han, Y.; Gu, M.; Kim, B.-S.; Ryu, J. Layer-by-Layer Assembly of Polyoxometalates for Photoelectrochemical (PEC) Water Splitting: Towards Modular PEC Devices. *ACS Appl. Mater. Interfaces* **2017**, *9*, 40151–40161.
- (32) Damrauer, N. H.; Cerullo, G.; Yeh, A.; Boussie, T. R.; Shank, C. V.; McCusker, J. K. Femtosecond Dynamics of Excited-State Evolution in [Ru(bpy)₃]²⁺. *Science* **1997**, *275*, 54–57.

(33) Choi, Y.; Ryu, G. H.; Min, S. H.; Lee, B. R.; Song, M. H.; Lee, Z.; Kim, B. S. Interface-Controlled Synthesis of Heterodimeric Silver-Carbon Nanoparticles Derived from Polysaccharides. *ACS Nano* **2014**, *8*, 11377–11385.

(34) Yu, H.; Shi, R.; Zhao, Y. F.; Waterhouse, G. I. N.; Wu, L. Z.; Tung, C. H.; Zhang, T. R. Smart Utilization of Carbon Dots in Semiconductor Photocatalysis. *Adv. Mater.* **2016**, *28*, 9454–9477.

(35) Toma, F. M.; Sartorel, A.; Iurlo, M.; Carraro, M.; Parisse, P.; Maccato, C.; Rapino, S.; Gonzalez, B. R.; Amenitsch, H.; Da Ros, T.; Casalis, L.; Goldoni, A.; Marcaccio, M.; Scorrano, G.; Scoles, G.; Paolucci, F.; Prato, M.; Bonchio, M. Efficient Water Oxidation at Carbon Nanotube-Polyoxometalate Electrocatalytic Interfaces. *Nat. Chem.* **2010**, *2*, 826–831.

(36) Folkman, S. J.; Finke, R. G. Electrochemical Water Oxidation Catalysis Beginning with Co(II) Polyoxometalates: The Case of the Precatalyst $\text{Co}_4\text{V}_2\text{W}_{18}\text{O}_{68}^{10-}$. *ACS Catal.* **2017**, *7*, 7–16.

(37) Kalyanasundaram, K. Photophysics, Photochemistry and Solar-Energy Conversion with Tris(Bipyridyl)Ruthenium(II) and Its Analogs. *Coord. Chem. Rev.* **1982**, *46*, 159–244.

(38) Artero, V.; Chavarot-Kerlidou, M.; Fontecave, M. Splitting Water with Cobalt. *Angew. Chem., Int. Ed.* **2011**, *50*, 7238–7266.